Sensitivity of an alkali-silica reaction kinetics model to diffusion and reactive mechanisms parameters

Guy-De-Patience Ftatsi Mbetmi, Stéphane Multon, Thomas de Larrard, Frédéric Duprat, Daniel Tieudjo

Sensitivity analysis of the parameters of a time-dependent alkali-silica reaction model

Guy-de-patience Ftatsi Mbetmi[a,b,1], Stéphane Multon[a], Thomas de Larrard[a], Frédéric Duprat[a], Daniel Tieudjo[c]

(a) *LMDC, Université de Toulouse, INSA, UPS, 135 Avenue de Rangueil, 31077 Toulouse cedex 04 France*

(b) **Laboratoire d'Analyses Simulations et Essais (LASE), Université de Ngaoundéré, IUT, P.O. Box 455, Ngaoundere, Cameroon**

(c) **Laboratoire de Mathématiques Expérimentales (LAMEX), Université de Ngaoundéré, ENSAI, P.O. Box 455, Ngaoundere, Cameroon**

Abstract: Alkali-silica reaction (ASR) expansion is due to a combination of chemo-mechanical mechanisms. To obtain realistic predictions, modelling developed at the material scale has to consider reactive transport and mechanical issues. Numerous input variables concerning aggregate and cement paste properties are thus necessary. The uncertainties that affect such variables make the prediction of the ASR phenomenon random and thus need to be considered in a probabilistic context. To reduce the stochastic dimension for a further probabilistic analysis, a sensitivity analysis using the Morris method is conducted here, at different dates, on an ASR model developed at the material scale. It is illustrated by a combined sensitivity analysis of both the total volume of ASR products formed over time and the corresponding expansion. The work shows the relative impact of transport and reactive mechanisms on ASR kinetics. Moreover, the most significant parameters are not the same for laboratory accelerated expansion tests as for real structures under low temperatures. This highlights the relative impact of ASR mechanisms according to temperature.

Keywords: Alkali-silica reaction (ASR), Sensitivity analysis, Monte Carlo simulation, Morris method, Reliability.

[1] guy.ftatsi@univ-ndere.cm

28

29 **Highlights:**

30 - A sensitivity analysis of alkali-silica reaction model parameters is performed,

31 - A method to compute multiple outputs sensitivity analysis is proposed,

32 - The method relies on using a cumulative frequency threshold value,

33 - ASR kinetics can be more sensitive to reactive mechanisms than to transport in old concrete,

34 - Environmental conditions impact the ranking of significant variables.

35

List of abbreviations and symbols

Agg.: Aggregates

ASR: Alkali-Silica Reaction

($\boldsymbol{B_{(k+1)\times k}}$): Lower triangular matrix

$\boldsymbol{cdfrq}$: cumulative decreasing frequency

CNA0 ($\boldsymbol{C_{Na}^{cp}}$): Initial concentration of alkali in cement paste

COLC ($\boldsymbol{t_c}$): Reaction rim thickness

CONGRA ($\boldsymbol{C_{agg}}$)**:** Volumetric concentration of aggregate per m^3 of concrete

D: Diameter

($\boldsymbol{D_{k\times k}^{*}}$): Diagonal matrix whose diagonal terms randomly take the values 1 or -1

DIFFG ($\boldsymbol{D}$): Alkali diffusion coefficients

EE: Elementary Effect

($\boldsymbol{\varepsilon_V(t)}$): REV ASR expansion over time

($\boldsymbol{f}$ **or** $\boldsymbol{Fixna}$): Coefficient of alkali fixation - taken as the same for all classes

FRAGRA(i): Fraction of the class i granular material in aggregates

($\boldsymbol{J_{(k+1)\times k}}$): Matrix of $(k+1)$ lines and k columns of ones

($\boldsymbol{k}$): Number of input variables

Max: Maximum

Min: Minimum

($\boldsymbol{\mu_i}$): Means on r of the EE_i

($\boldsymbol{\mu_i^*}$): Absolute means on r of the EE_i

($\boldsymbol{p}$): Number of levels of each variation range (with $p > k$)

($\boldsymbol{\phi_{ai}}$): Fraction of aggregate of class i

($\boldsymbol{P^*_{k\times k}}$): Matrix where each column and each line contain only one element equal to 1 and all the others are equal to 0

POROG ($\boldsymbol{P_{agg}}$): Porosity of aggregates

POROMO: Porosity of the cement paste

($\boldsymbol{r}$): Number of trajectories

($\boldsymbol{R}$): The ideal gas constant

($\boldsymbol{R_{ai}}$): Radius of aggregate of class i

REV: Relative Elementary Volume

RH: Relative Humidity

RNS: Number of mol of Na reacting with 1 mol of Si to form 1 mol of gel

($\boldsymbol{S_i^*}$): Global sensitivity indices of each variable

($\boldsymbol{\sigma_i}$): Standard deviation on r of the EE_i

SILSOL: Amount of soluble silica

($\boldsymbol{S_{thv}}$): Sensitivity threshold value

($\boldsymbol{T}$): Temperature

($\boldsymbol{T_0}$): Reference temperature of the LPC N° 44 test ($311\ ^\circ K$)

($\boldsymbol{V_{g(t)}}$): Total volume of gel formed over time

VMGEL ($\boldsymbol{V_{gel}^{mol}}$): Molar volume of ASR-created gel

($\boldsymbol{Vn[l]}$): Levels vector

($\boldsymbol{V_{por}}$)**:** Rim volume surrounding reactive particles

($\boldsymbol{X_{max}^i}$): Maximum values of variables X_i with $i = 1, .., k$

($\boldsymbol{X_{min}^i}$): Minimum values of variables X_i with $i = 1, .., k$

1. Introduction

Alkali-aggregate reaction causes significant deleterious degradation in many concrete structures, especially those where the concrete saturation degree is permanently high, such as dams. The alkali-aggregate reaction studied here is the alkali-silica reaction (ASR). It takes place between the poorly crystallized siliceous phases of silica aggregates and the alkaline interstitial solution of concrete. This reaction results in the formation of a gel and / or crystallized products, which can pressurize the surrounding concrete, causing cracking and expansion. Modelling ASR at the material level involves the transport of ionic species in the aggregate, the reactive mechanisms of dissolution and precipitation, and the conservation of ionic masses. During the reactive processes, silanol and siloxane interact to create siliceous gels [1–3]. ASR models must take both chemical and physical aspects into account to obtain relevant predictions of the mechanical responses of affected structures.

Apart from the approximations associated with the accepted hypothesis, many uncertainties affect the variables of the model, make the prediction of the ASR phenomenon random, and require operations to be carried out in a probabilistic context. A recent study proposed by Saouma pointed out the importance of stochastic analysis for the evaluation of ASR-damaged dams [4]. A similar situation exists for the determination of the advancement of the reaction according to environmental conditions in order to obtain accurate assessment of the evolution of damage with time. For the purpose of probabilistic analysis of the functional reliability of dams, a methodology based on the use of surrogate models has been planned for further study. The model adopted in the present work is the one developed at the material scale in LMDC by Multon et al. [5]. It has been compared with experimental evidence in [6]. To reduce the large number of variables to be considered as random in a probabilistic context, a one-at-a-time sensitivity analysis is undertaken. The final number of variables resulting from the reduction process is called the effective dimension, a concept introduced by Paskov and Traub [7] in finance, then by Caflisch et al. [8] in engineering. Later on, Kucherenko et al. [9] proposed the use of global sensitivity analysis with Sobol indices to obtain a model effective dimension. Riahi [10] developed an approach that consists of calculating the stochastic effective dimension with the Morris method. The present work extends that approach to multiple outputs and time dependent sensitivity analysis. The Morris method is used here to reduce the stochastic dimension, and so the computational cost, of our model rather than enhancing its predictive capabilities as in [11]. Additionally, we combine the sensitivity analyses performed at different dates to consider the time-dependency of the model in the present study.

Before the description of the ASR model used in this paper, a review of ASR modelling is proposed, followed by a presentation of the variation range of each input variable obtained with some Monte Carlo simulations to fit the experimental results of the ASR accelerated test LPC N° 44 [12–15], carried out on cores drilled from Song Loulou dam in Cameroon [16] thirty years after its commissioning. Then, the Morris method is presented and an algorithm proposed to select variables on the basis of a combined sensitivity analysis. Finally, the sensitivity study is carried out on the selected model outputs. The most important variables are identified for each of the outputs, and from the combined sensitivity analysis, for different environmental conditions.

2. Modelling Alkali-Silica Reaction at material scale

2.1. Literature review

Alkali-Silica Reaction is caused by the chemical attack of specific silica aggregates and results in expansion and cracking of concrete. ASR modelling is thus an ambiguous term as the different models found in the literature can be centred on different aspects of physics. Some numerical works focus on mechanical considerations [17–25], some others analyse only the chemical advancement [26–31], while a third type of works consider the combination of physico-chemical mechanisms with mechanical considerations [5, 32–38]. To be realistic, ASR modelling should take into account:

- Transport for ions, water and ASR gels [5,26,28–30,32–38]: Before attacking aggregate, hydroxyl ions have to come into contact with amorphous silica (diffusion of ions in cement paste and aggregate). The ion diffusion is only possible if the porosity is sufficiently saturated in water and, to form, ASR gels absorb water (effect of water diffusion and permeability in concrete). Once formed, ASR gels under pressure just after their formation can partially move into the concrete porosity and induce cracking (ASR gel permeation).
- Thermodynamics [27,28,31]: ASR is the result of the aggregate dissolution (reaction between hydroxyl ions and amorphous silica) and of the precipitation of gels (reaction between silicic acid and alkali). These chemical reactions can be modelled by thermodynamic equilibrium [27,28] or by kinetics laws [5,39,40].
- Mechanics [5,17,18,20–25,32,41–43]: The formation of ASR gels in hardened concrete leads to cracking and expansion. Fracture or damage mechanics is necessary to evaluate the mechanical properties after degradation. Concrete creep has to be taken into account as it impacts the development of cracking.

In the literature, ionic or water transports are often considered as the processes controlling ASR kinetics. Recent works [28,39] have shown the importance of considering both transport and the

kinetics of chemical reactions to obtain realistic representations of rapid and slow reactive aggregate, e.g. the attack pattern observed in the literature [44]. Therefore, ASR modelling at material scale should be performed in a reactive transport framework. This leads to modelling with numerous input data. These data are affected by uncertainties and the prediction of ASR by such modelling is thus a random phenomenon. A probabilistic context can help to obtain reliable predictions. Among the few models eligible for the new approach that we intend to develop, namely the recalculation of ASR-affected structures from a microscopic model based mainly on measurable physical parameters, we chose the ASR model presented in [5] as it combines transport and reactive mechanisms.

2.2. Physico-chemical ASR modelling

2.2.1 General modelling

The ASR model used in this work considers the definition of a representative elementary volume (REV) of concrete that contains both cement paste and aggregate particles, reactive or not, of different sizes (Fig. 1). The REV is the smallest volume that represents the behaviour of the real concrete volume. Geometrical parameters thus have a large place in this modelling to characterize the size of reactive aggregates (minimal diameter of an aggregate class, DMIN and maximal diameter, DMAX) and the aggregate distribution (volumetric aggregate concentration – CONGRA, and fractions of each aggregate size – FRAGRA) presented in Table 1. Three granular classes are considered and the number (a) in Table 1 is associated with the aggregate class ($a = 1,2,3$).

The model developed at LMDC is based on the following chemical mechanisms:

- the diffusion of alkali into the aggregate particles (Fig. 1). Only one transport mechanism is considered. It is sufficient to reproduce a large number of experimental tests in saturated conditions [5,6,39]. For this part, the parameters of the model are the initial alkali concentration (CNA0), the aggregate porosity (POROG) and the coefficient of diffusion of alkali in aggregate (DIFFG) in Table 1.

- production of ASR gel (Fig. 1) and decrease of the alkali concentration in the cement paste relatively to their consumption by the new products to represent the reactive mechanisms. The maximal number of moles produced by ASR depends on the initial content of reactive components (the alkali concentration – CNA0 and the reactive silica content in aggregate – SILSOL) and on the ratio Na_2O_{eq}/SiO_2 in the gel (RNS in Table 1). The gel volume is

proportional to the number of gel moles and to the molar volume of ASR gels (VMGEL). The kinetics of gel production is driven by the coefficient of alkali fixation (FIXNA), which quantifies the fixation of alkali by the gel and thus the creation of gel.

- permeation of gels around reactive sites in aggregate and paste porosity [32] and formation of rims around reactive aggregate [45]. For the sake of simplicity, the volume of gels filling pores and the volume of gels necessary to form the rims are modelled by an equivalent thickness (COLC) between cement paste and aggregate (Fig. 1). In reality, this volume of gel is accommodated in all the pores available in the aggregate and surrounding cement paste. In the rim, the porosity of the cement paste (POROMO) is assumed to be partly filled by gels. The gel produced once the rim is formed exerts significant pressure on the surrounding aggregate and cement paste and causes the REV expansion and cracking.

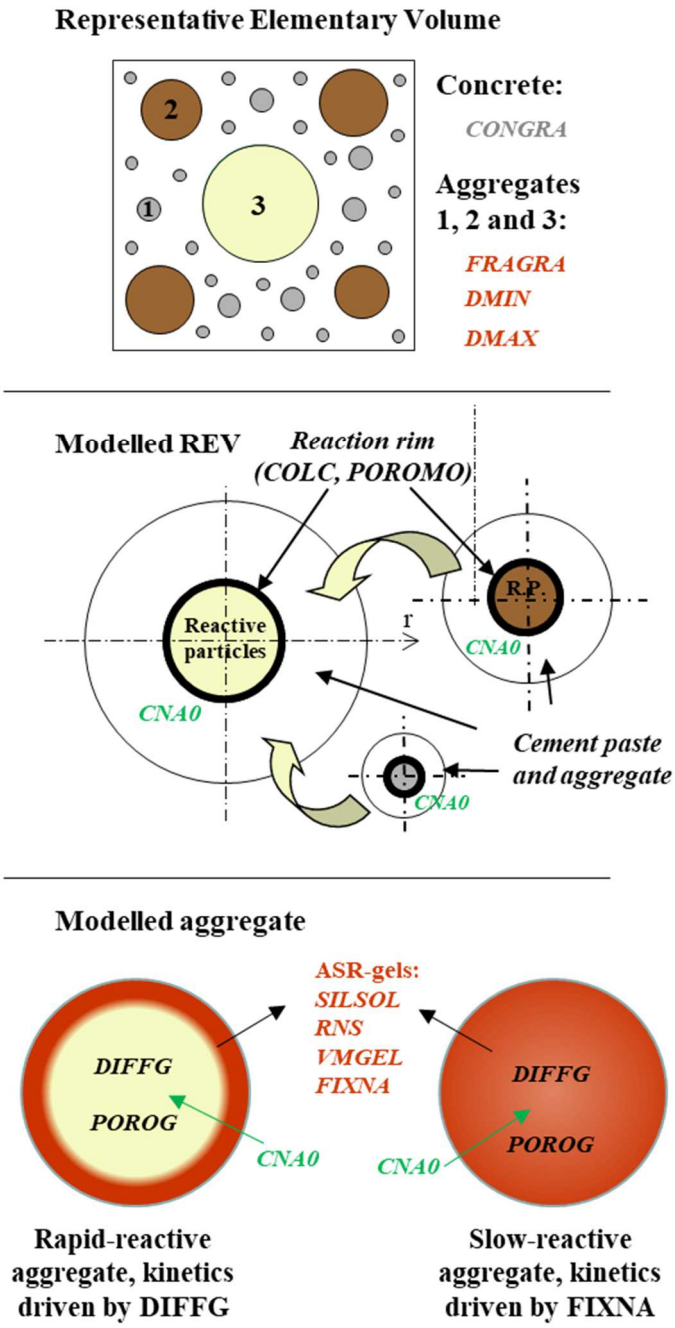

193

194 **Fig. 1.** Definition of the Relative Elementary Volume [5] and model parameters

195

196

197

198

Table 1. Ranges of variations of the input variables of the model

Concrete Parameters					
Description	**Abbreviation**	**Symbol** [5]	**Initial Range**	**Final Range**	**Unit**
Minimum diameter of the smallest granular class	DMIN(1)	$R_{(a=1,2,3)}$ = (DMIN(a) + DMAX(a)) / 2	0 to 2	0 to 2	mm
Minimum diameter of the intermediate granular class	DMIN(2) = DMAX (1)		4 to 6	4 to 6	mm
Minimum diameter of the largest granular class	DMIN(3) = DMAX (2)		10 to 20	10 to 20	mm
Maximum diameter of the largest granular class	DMAX(3)		32 to 125	32 to 125	mm
Volumetric concentration of aggregate per m³ of concrete	CONGRA	C_{agg}	0.6 to 0.75	0.6 to 0.75	-
Fraction of the smallest granular class in aggregates	FRAGRA(1)	$\phi_{(a=1,2,3)}$ = *Function of* (FRAGRA(a), SILSOL(a))	0.25 to 0.55	0.25 to 0.55	-
Fraction of the medium and large granular class in aggregates	FRAGRA(2) = FRAGRA(3)		0.05 to 0.25	0.05 to 0.25	-
Physicochemical Parameters					
Description	**Abbreviation**	**Symbol** [5]	**Initial Range**	**Final Range**	**Unit**
Initial concentration of alkali in cement paste	CNA0	C_{Na}^{cp}	**100 to 800**	**100 to 250**	mol/m³
Amount of soluble silica for the smallest granular class (Sand)	SILSOL(1)	$\phi_{(a=1,2,3)}$ = *Function of* (FRAGRA(a),SILSOL (a))	**1000 to 5000**	**1000 to 3000**	mol/m³ of aggr.
Amount of soluble silica taken for the other granular classes and average reactivity	SILSOL(2) = SILSOL(3)		**1000 to 5000**	**1000 to 3000**	mol/m³ of aggr.
Porosity of the cement paste	POROMO	P_{cp}	0.1 to 0.3	0.1 to 0.3	-
Porosity of small aggregates	POROG(1)	P_{agg1}	0.01 to 0.05	0.01 to 0.05	-
Porosity of aggregates taken for the other granular classes	POROG(2) = POROG(3)	$P_{agg2,3}$	0.01 to 0.05	0.01 to 0.05	-
Reaction rim thickness for small aggregates	COLC(1)	$t_{c(a=1)}$	**1 to 15**	**1 to 10**	µm
Reaction rim thickness for other aggregates	COLC(2) = COLC(3)	$t_{c(a=2,3)}$	**1 to 15**	**1 to 10**	µm
Alkali diffusion coefficients for small aggregates	DIFFG(1)	$D_{(a=1)}$	2.10^{-13} to 7.10^{-13}	2.10^{-13} to 7.10^{-13}	m²/s
Alkali diffusion coefficients for other aggregates	DIFFG(2) = DIFFG(3)	$D_{(a=2,3)}$	2.10^{-13} to 7.10^{-13}	2.10^{-13} to 7.10^{-13}	m²/s
ASR gel parameters					
Description	**Abbreviation**	**Symbol** [5]	**Initial Range**	**Final Range**	**Unit**
Molar volume of ASR-created gel	VMGEL	V_{gel}^{mol}	**1.10^{-5} to 10.10^{-5}**	**1.10^{-5} to $1.6.10^{-5}$**	m³/mol
Number of mol of Na reacting with 1 mol of Si to form 1 mol of gel	RNS	*Ratio Na_2O/SiO_2*	**0.2 to 0.8**	**0.39 to 0.59**	-
Coefficient of alkali fixation taken as the same for all classes	FIXNA	f	-1.10^{-7} to -1.10^{-9}	-1.10^{-7} to -1.10^{-9}	m³/m³/s

The constitutive equations of the ASR gel expansion model have been presented and explained in [5]. Both rapid and slow reactive aggregates can be modelled (Fig. 1) through the combination of

diffusion and reactive mechanisms [39]. Only one point has been modified from the initial version of the model [5]: the existence of a constant threshold alkali concentration above which ASR can occur is questionable [39,46]. This threshold is probably dependent on chemical conditions, e.g. calcium concentration [39]. In the present work, no alkali concentration threshold is assumed. All the alkali ions can participate in gel formation.

The input variables analysed in this paper are all summarized in Fig. 1 and Table 1. The ranges were derived from our expertise combined with the information available in the literature, as explained in the next section. It can be deemed that they contain about 95% of the consistent knowledge of the parameters in question, as justified in part 2.3.

2.2.2 Consideration of environmental conditions

In the model, the temperature impacts both the transport, through the alkali diffusion coefficient in the aggregate, and the reactive mechanisms (dissolution of silica and ASR-gel formations), through the single simplified equation of alkali fixation [39]. As shown by the literature, reactive mechanisms are usually more sensitive to temperature than diffusive transport [27,47,48]. This is taken into account through the activation energy of each phenomenon, $E_A^{Fixna} = 78$ kJ/mol for the alkali fixation (Eq. 1), versus $E_A^{DiffG} = 20$ kJ/mol for the alkali diffusion (Eq. 2).

$$Fixna\,(T) = Fixna_0\, e^{\frac{E_A^{Fixna}}{R}\left(\frac{1}{T}-\frac{1}{T_0}\right)} \quad \text{(Eq. 1)}$$

$$DiffG\,(T) = DiffG_0\, e^{-\frac{E_A^{DiffG}}{R}\left(\frac{1}{T}-\frac{1}{T_0}\right)} \quad \text{(Eq. 2)}$$

where $R = 8.31\,J.K^{-1}.mol^{-1}$ the ideal gas constant; T ($°K$), temperature; $T_0 = 311\,°K$, temperature of the expansion test performed on cores (LPC N° 44), test taken as a reference in this work.

The variation of relative humidity can be considered in the modelling through the variation of the diffusion coefficient with the saturation degree of the concrete [49]. The impact of the variation of moisture on the model response has not been evaluated in the paper because the specimens during the accelerated test (RH 95%) and the concrete of the Song Loulou dam (RH > 80%) [50] were at very high and quasi-constant relative humidity during ASR expansion. Concerning the alkali effect on expansion, alkali leaching can occur during the expansion test and can be considered by the modelling [39]. However, the cores extracted from the concrete of the Song Loulou dam had a

diameter of 140 mm. Therefore, alkali leaching was neglected as Lindgård et al. showed that the loss of alkali was lower than 10% for specimens with sizes greater than 100 mm [51].

2.3. Independent input variables of the model and range of variation

Following a study commissioned by the dam manager, core specimens were drilled from the Song Loulou hydropower dam (Fig. 2), to undergo various tests including the accelerated swelling test LPC N°44 and the petrographic study carried out by the former LCPC (Laboratoire Central des Ponts et Chaussées) in 2011. LPC N°44 is an expansion test on a core extracted in an ASR-affected concrete structure. The core had to be equipped with plots for strain measurement and kept in a 38 °C and 95% RH environment. The evolution of the length had to be noted regularly over 52 weeks [12]. In order to obtain homogeneous conditions, cores are usually stored in small containers (28 cm x 23 cm x 40 cm in height) [13].

The cores presented in Fig. 2 were extracted from the following points of the Song Loulou dam: at the base of buttress 45 (C45-1), on the top of spillway pile 12 (P12-1), on the right bank of the spillway pile (P12-2).

Fig. 2. Cores extracted from Song Loulou dam for the LPC N° 44 test, credit to Guedon - IFSTTAR 2010

For our sensitivity analysis to be relevant using the proposed method, it is necessary to define the real ranges of the independent input variables. Twenty of them have been identified for the model, (**Table 1**), considering that the smallest granular class (sand) has different physicochemical properties from the middle and large classes (gravel and stones). This hypothesis is based on the dam construction data and the 2011 petrographic observations. Additionally, in the case of cores

253 drilled from the structures, aggregates had already been attacked in the structure, before the
254 laboratory tests. Due to diffusive mechanisms, the chemical advancement in sand is potentially
255 larger than the advancement in gravel and stones, inducing different physicochemical properties.

256 The initial ranges of the input variables were defined according to literature and Song Loulou dam
257 construction reports. The first 7 variables in **Table 1** are physical variables whose ranges were
258 deduced from the concrete formulation of the Song Loulou dam, and also in accordance with [52].
259 The porosity range was measured on extracted cores. The initial ranges of the twelve other
260 variables were defined from the literature [5,6,34,53]. In addition to these three references used for
261 all the variables, we used specific references for some variables: values for the initial alkali
262 concentration, "CNA0" and the molar volume of ASR gels, "VMGEL" were from [54] and, for
263 the two coefficients of alkali diffusion in aggregate "DIFFG", the values were from [47].

264 These ranges were then refined by using Monte Carlo simulations [55,56], in order to reflect the
265 reality of our study case. For that purpose, on the basis of the results obtained from tests carried
266 out on ten cores [16], three reference data were selected: P12-1 and P12-2 were drilled in Pier 12
267 of the dam and represent the minimum and the average kinetics respectively (Fig. 3), C45-1 was
268 drilled from the basis of Buttress 45 and represents the maximal ASR kinetics obtained for the
269 expansion tests performed on the concrete dams. Some 2000 simulations to approach the final
270 intervals were run by progressively reducing the initial intervals. Then 10 000 simulations were
271 performed to confirm the ranges which best fit the experimental curves. It is important to note that
272 the intervals of the variables deduced from Song Loulou construction expansion tests were kept
273 constant during the process. The aim of the procedure is that the 95% confidence interval should
274 frame the extreme experimental values (Fig. 3). The final ranges used in the sensitivity analysis
275 below are shown in Table **1**. The statistics computed from the Monte Carlo simulations show that
276 the experimental values are well within the 95% confidence interval of results from the model
277 (Fig. 3). The final ranges given in Table **1** can be useful to evaluate the potential expansion of
278 concrete damaged by ASR with similar characteristics.

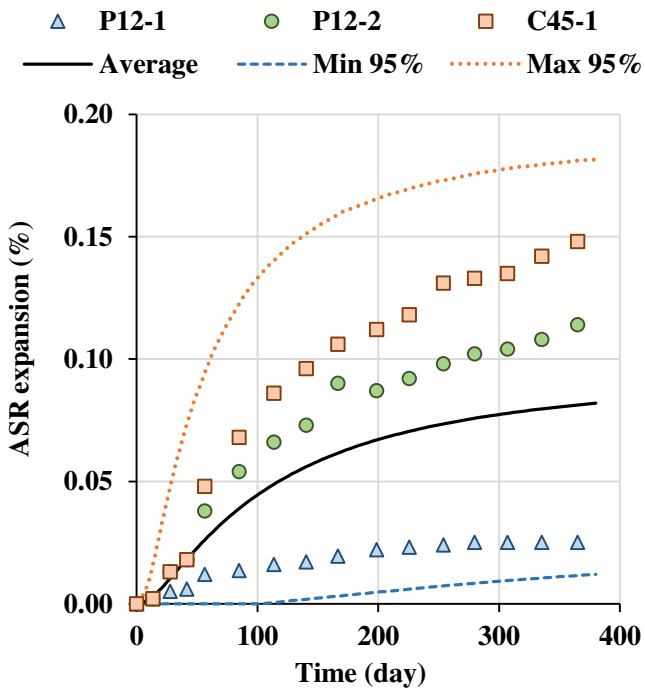

279

280 **Fig. 3.** Kinetics of minimal, average and maximal swelling for a quantile of 95% - 10 000
281 simulations - Final ranges (dots: experimental data, lines: model)

282 ## 3. Morris method and variable selection algorithm

283 The Morris method [57–59] allows input variables to be classified according to their importance
284 with regard to their influence on the response of a model. It is based on the assumption that, by
285 varying variables of the same relative pitch one at a time, the one that causes the greatest variation,
286 expressed in statistical terms, on the output is the most important. The process results in the
287 stochastic dependence between variables not being taken into account. So, to use that method,
288 variables need to be independent.

289 ### 3.1. Trajectories and Elementary Effects (EE)

290 The first step is to construct trajectories that will be used to calculate the elementary effects and
291 the Morris sensitivity analysis indicators. For that purpose, we divide the variation range of each
292 of the k input variables into p levels ($p > k$) from the minimum to the maximum with a pitch (or
293 perturbation $\Delta = 1 / (p - 1)$. Then, we build r trajectories each consisting of $k + 1$ points and
294 their respective responses. The first point is drawn randomly and the other k points are calculated
295 so that just one of the k variables changes by $\pm \Delta$ from one calculated point to another. Each
296 trajectory is used to determine an Elementary Effect (EE) of each variable according to the
297 expression (Eq. 3)

$$EE_i = f(X_1, \dots, X_i + \Delta, \dots X_k) - f(X_1, \dots, X_i, \dots X_k)/\Delta \quad \text{(Eq. 3)}$$

The computation of the Morris indicators requires several elementary effects per variable and therefore the computation of several trajectories. Fig. 4 shows five trajectories for two variables ($r = 5, k = 2$), with the expressions of some of the resulting elementary effects. The first point of each of these trajectories is drawn randomly and the other two points ($k + 1 = 3$ points per trajectory) are computed in order to have only one relative variation of ± Δ between two consecutive points.

Generally, a trajectory can be constructed by matrix computation according to equations (Eq.4) and (Eq.5), the details of which are given in [59]. However, a clear description of the constitutive elements of these equations is given in the algorithm in **Appendix A**.

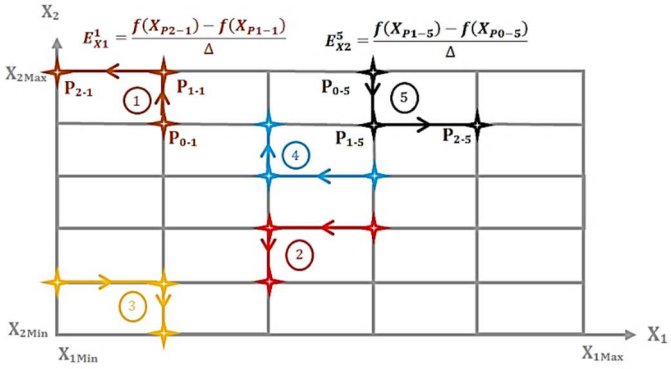

Fig. 4. Example of elementary effects for $\boldsymbol{k = 2, r = 5, p = 6}$ ($\boldsymbol{\Delta = 0.2}$)

$$B^*_{(k+1)\times k} = J_{(k+1)\times 1} \,.\, X^*_{1\times k} + \left(\Delta/_2\right) . \left[\left(2B_{(k+1)\times k} - J_{(k+1)\times k}\right) . \, D^*_{k\times k} + J_{(k+1)\times k}\right] . \, P^*{}_{k\times k} \quad \text{(Eq.4)}$$

The points of the trajectory are given by:

$$X^{i,j}_{i=1,2,\dots,k+1;j=1,2,\dots,k} = X^j_{min} + B^*_{i,j}\left(X^j_{max} - X^j_{min}\right) \quad \text{(Eq.5)}$$

3.2. Sensitivity analysis indicators and selection of variables

Sensitivity analysis indicators are computed from elementary effects statistics, equation (Eq.*6*) from *[58]*, and equation (Eq.7) deduced from *[60]*. μ_i and σ_i are respectively the mean value and standard deviation of the elementary effects. μ_i^* is the mean value of the absolute elementary effects. High values of μ_i^* reveal a strong sensitivity to the variables considered and σ_i is related to non-linear aspects. S_i^* is an indicator of global sensitivity. The number of trajectories required is

that from which these indicators become constant. The larger that number is, the more accurate are the results, but the calculation cost also increases.

$$\mu_i = \sum_{j=1}^{r} EE_{i,j}/r,\ \mu_i^* = \sum_{j=1}^{r} \left|EE_{i,j}\right|/r\ ,\ \sigma_i = \sqrt{\frac{1}{(r-1)} \times \sum_{j=1}^{r} (EE_{i,j} - \mu_i)^2} \quad \text{(Eq.6)}$$

$$S_i^* = (\mu_i^{*2} + {\sigma_i}^2)/\sum_{i=1}^{n} \left(\mu_i^{*2} + {\sigma_i}^2\right) \quad \text{(Eq.7)}$$

3.3. Variables selection algorithm

The selection process used in the present study is summarized in the Algorithm in Appendix A. For a single output, the variables for which the cumulative decreasing global sensitivity indices are lower than a threshold value will be selected. For multiple outputs, we sum the global sensitivity indices of each variable on all outputs and compute the cumulative decreasing frequency of each sum. Then the variables with a cumulative decreasing frequency less than a threshold value are selected. Commonly, the threshold values used in sensitivity analysis are either 90%, for a narrow selection window, or 99%, for a large selection window. In the applications given in the following parts, a medium sized selection window with a threshold value of 95% is chosen.

4. Sensitivity analysis of the ASR model during accelerated expansion test

The ASR model developed in the LMDC [5] can be used to evaluate the production of gel during LPC accelerated test N° 44 on a test specimen. Tests are carried out at 38 °C and 100% relative humidity. Using the Morris method with the parameters $k = 20, r = 600, p = 81$ ($\Delta = 0.0125$), the respective variation ranges for the input variables on various outputs of interest deduced from the model (Table **1**) are considered. Values of r and p lead to an accurate sensitivity analysis. Let us recall that we used three granular classes when implementing the model, where digits 1, 2 and 3 are associated with small, medium and large sizes respectively. The sensitivity of the model is first analysed according to the two main outputs:

- the total volume of gel formed during time **t**:

$$\boldsymbol{V_g(t)} = \sum_{\boldsymbol{i=1}}^{\boldsymbol{3}} \boldsymbol{V_{gi}(t)} \quad \text{(Eq.8)}$$

- and the corresponding ASR expansion evaluated in this work by the following equation:

$$\boldsymbol{\varepsilon_V(t)} = \sum_{\boldsymbol{i=1}}^{\boldsymbol{3}} \frac{\boldsymbol{V_{gi}(t) - V_{por\_i}}}{\boldsymbol{V_{VERi}}} \quad \text{(Eq.9)}$$

with V_{por}, the rim volume surrounding reactive particles [5].

The first output is related to the chemical aspects of ASR, while the second output is the one that effectively impacts the mechanical behaviour of the concrete.

4.1. Sensitivity of the total volume of gel formed during time Vg (t)

4.1.1 Sensitivity analysis at different dates

The analysis of the sensitivity of the total volume of gel formed during time (Vg (t)) was performed for 4 different dates: 10, 100, 180, and 365 days after the beginning of the test, in order to regularly cover the ASR accelerated test duration. Fig. 5 shows the results obtained at 365 days. The five variables that can be considered important, since their cumulative decreasing global sensitivity index is less than or equal to 95% (S_{thv} = 95%) are those represented by the dark bars on the histogram of Fig. 5: the coefficient of alkali fixation (FIXNA), the size of the biggest aggregate (DMAX(3)), the initial alkali concentration (CNA0), the coefficient of diffusion of the biggest aggregate (DIFFG(2)=DIFFG(3)) and the molar volume of ASR gels (VMGEL). Fig. 6 shows the ranking of the important variables for each of the four dates.

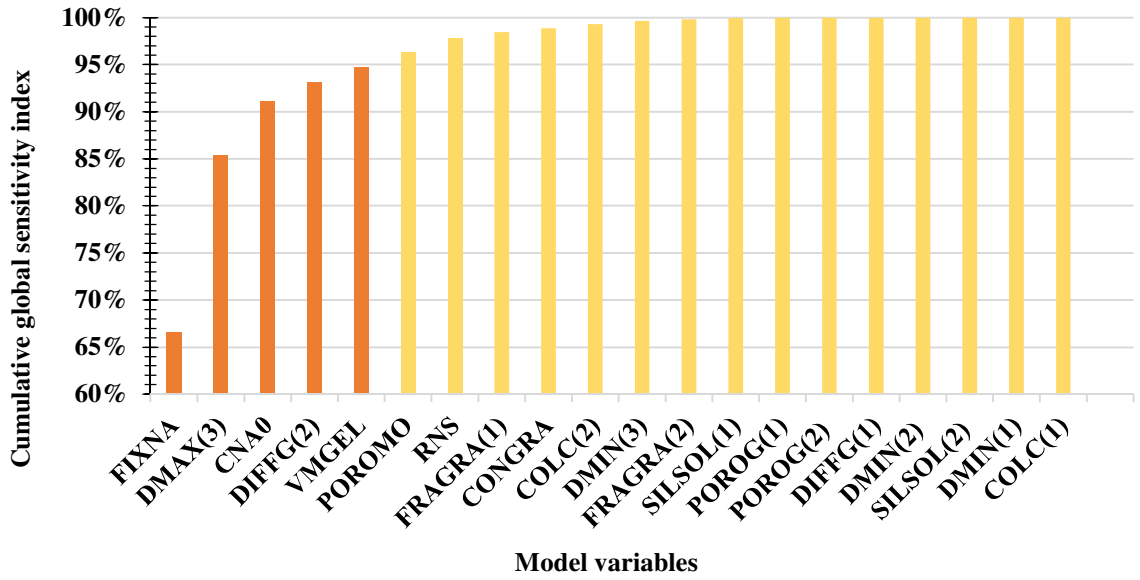

Fig. 5. Global cumulative sensitivity index of $\boldsymbol{V_g(t = 365\ days)}$

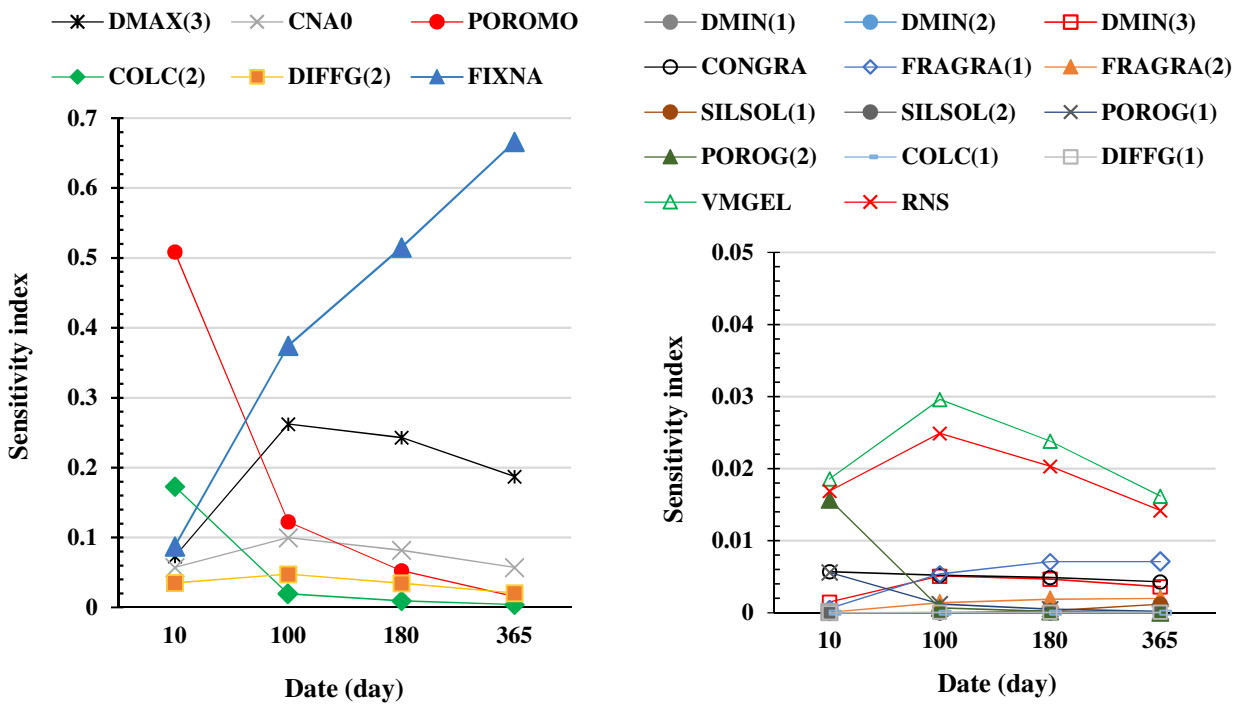

Fig. 6. Global sensitivity index for $V_g(t)$ at different times: parameters with high sensitivity (a) and parameters with sensitivity lower than 0.04 for all times (b)

One remarkable fact is that both the thickness of the reactive rim for medium and large aggregates, namely "COLC(2)", and the porosity of the mortar "POROMO", which appear to be important at 10 days (i.e. at the initialization of the reaction), become less important with time. This highlights the importance of these two parameters in the latency time of expansion (at the beginning, ASR gels can migrate in the porosity close to the reactive sites without inducing expansion). Conversely, the size of the largest aggregate, "DMAX(3)", is less important at the beginning of expansion than later. At the beginning of expansion, alkali has not had time to reach the reactive silica in the largest aggregates and they cannot produce gels.

The global sensitivity index of the alkali fixation coefficient "FIXNA" increases throughout the period. This can be physically justified by the fact that the alkali diffusion phenomenon, which is dominant in the beginning of the ASR reaction, gradually decreases, giving way to alkali fixation by the gel. The two other important variables ("DIFFG(2) " and "CNA0") have almost constant sensitivity during the test period.

379

380 *4.1.2 Global indicator for sensitivity analysis for the whole period*

381 As shown just above, the sensitivity of each parameter varies with time. It can be useful to
382 combine the sensitivity at the different times in a single, global indicator. Thus, the parameter with
383 the greatest impact during the whole period of expansion can be highlighted.

384 For each variable, the indicator is equal to the sum of the Morris global sensitivity at all dates
385 investigated:

$$\sum_t S_i^{Vg(t)} = S_i^{Vg(10)} + S_i^{Vg(100)} + S_i^{Vg(180)} + S_i^{Vg(365)} \quad \text{(Eq.10)}$$

386 The results are presented in Table 2. A corresponding frequency can be deduced by using the
387 relative global sensitivity:

$$frq = 100 \frac{\sum_t S_i^{Vg(t)}}{\sum_i \left(\sum_t S_i^{Vg(t)} \right)} \quad \text{(Eq.11)}$$

388 The variables are sorted in decreasing order compared to this last indicator. The fourth column of
389 Table 2 indicates the cumulative frequency, $cdfrq$, leading to the selection of the most influential
390 variable for the whole period of expansion. The most influential variables have a $cdfrq \leq S_{thv} =$
391 95%. They are highlighted in Fig. 7.

392

Table 2. Cumulative frequency on the sum of global sensitivity index of V_g for all dates

Description	$\sum_t S_i^{V_g(t)}$	frq (%)	$cdfrq$ (%)	S.V.
DMIN(1)	0.000	0.000	**41.075**	**FIXNA**
DMIN(2)	0.000	0.000	**60.215**	**DMAX(3)**
DMIN(3)	0.015	0.373	**77.708**	**POROMO**
DMAX(3)	0.766	19.140	**85.115**	**CNA0**
CONGRA	0.020	0.503	**90.273**	**COLC(2)**
FRAGRA(1)	0.020	0.505	**93.725**	**DIFFG(2)**
FRAGRA(2)	0.005	0.135	95.930	VMGEL
CNA0	0.296	7.408	97.838	RNS
SILSOL(1)	0.002	0.038	98.343	FRAGRA(1)
SILSOL(2)	0.000	0.000	98.845	CONGRA
POROMO	0.700	17.493	99.260	POROG(2)
POROG(1)	0.007	0.187	99.633	DMIN(3)
POROG(2)	0.017	0.415	99.820	POROG(1)
COLC(1)	0.000	0.000	99.955	FRAGRA(2)
COLC(2)	0.206	5.158	99.993	SILSOL(1)
DIFFG(1)	0.000	0.007	100.000	DIFFG(1)
DIFFG(2)	0.138	3.453	100.000	DMIN(1)
VMGEL	0.088	2.205	100.000	DMIN(2)
RNS	0.076	1.908	100.000	SILSOL(2)
FIXNA	1.643	41.075	100.000	COLC(1)

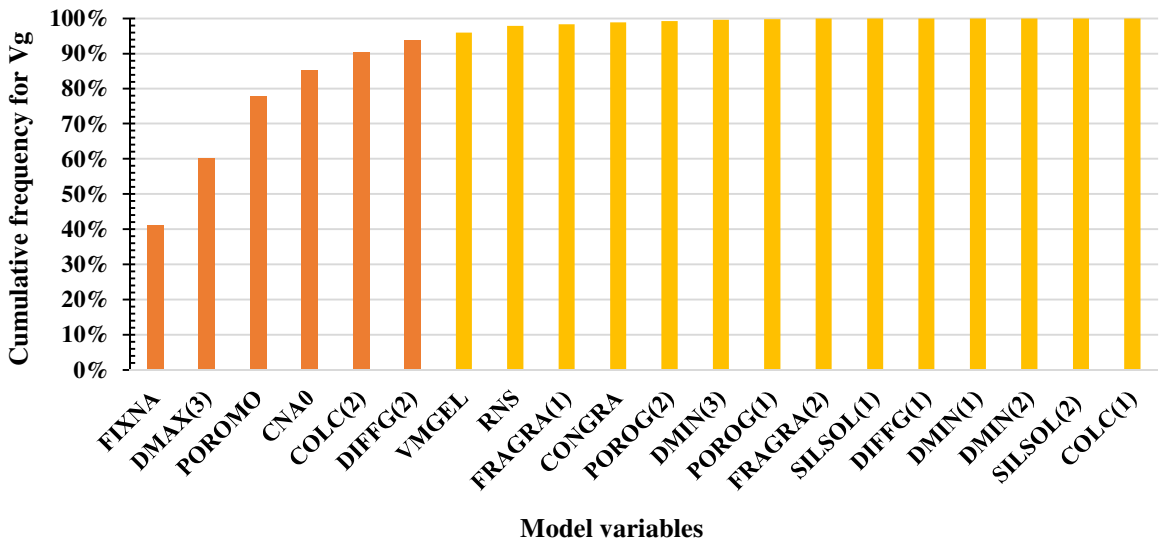

Fig. 7. Cumulative frequency for $\boldsymbol{V_g}$ for the whole period

The most influential variables on ASR gel creation quantified by V_g would be: the coefficient of alkali fixation "FIXNA", the maximum diameter of the largest granular class "DMAX(3)", the

mortar porosity "POROMO", the initial concentration of alkali in cement paste "CNA0", the rim thickness for medium and large sized aggregates "COLC(2)" and the coefficient of alkali diffusion for medium and large sized aggregates "DIFFG(2)".

4.2. Results for the corresponding REV expansion during time $\varepsilon_V(t)$

4.2.1 Sensitivity analysis at different dates

The same procedure was used for the second output, namely the ASR expansion during time, $\varepsilon_V(t)$, for the same 4 dates as in the previous section. Fig. 8 summarizes the outcome of the sensitivity analysis at the four chosen dates.

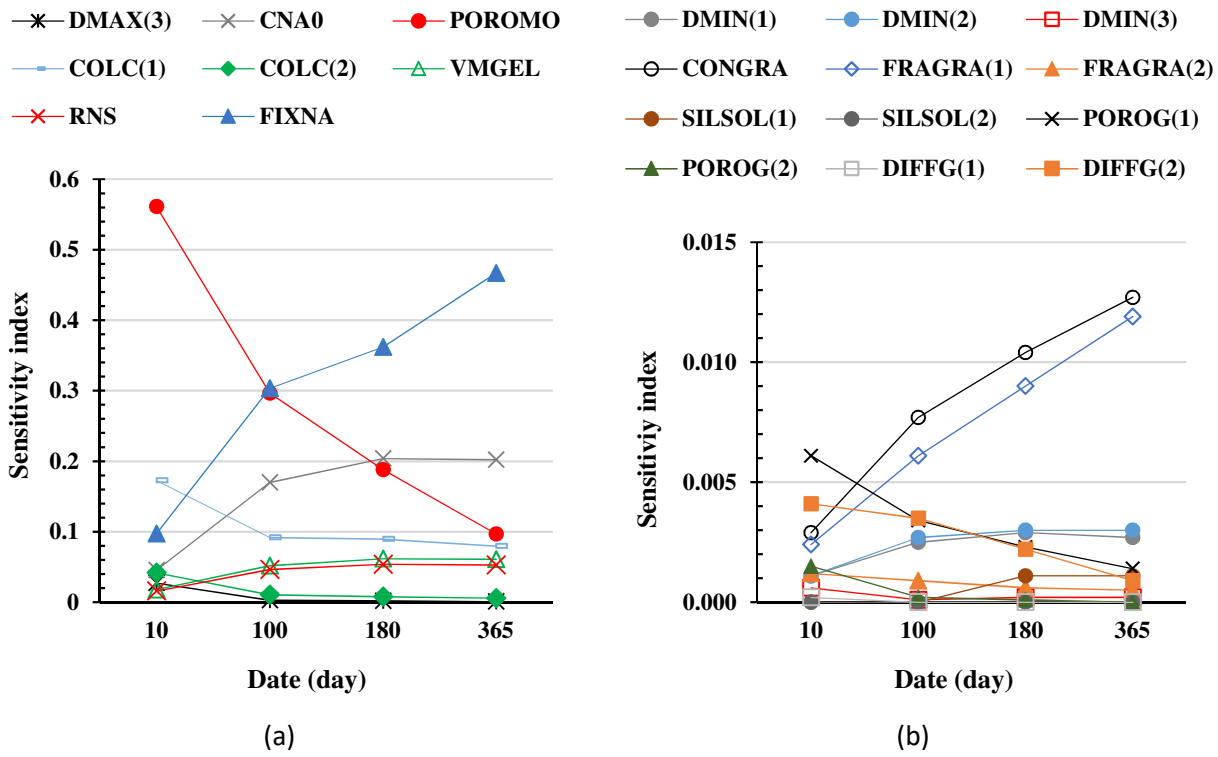

Fig. 8. Global sensitivity index of ASR expansion, $\varepsilon_V(t)$, at different times: parameters with the highest sensitivity (a) and parameters with sensitivity lower than 0.015 for all times (b)

We can observe the same result concerning "POROMO" and "FIXNA" as in the previous paragraph. Given that ε_V is REV relative data, the fact that small (respectively big) aggregates have small (respectively big) REV volume as the divisor might explain why the maximum diameter of the largest granular class DMAX(3), which appears to be important in the analysis of $V_g(t)$, disappears in the analysis of ε_V.

4.2.2 Global indicator for sensitivity analysis

After using the same procedure as for $V_g(t)$ with the data presented in Fig. 8, we obtained the overall result presented in Fig. 9 for the four dates.

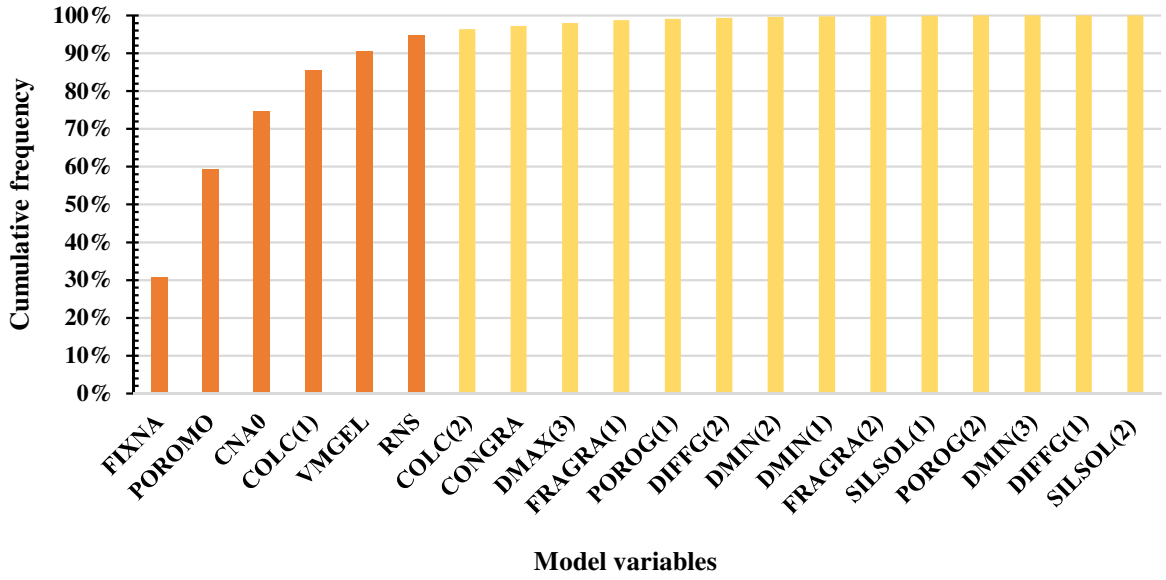

Fig. 9. Cumulative frequency on the sum of global sensitivity index of ASR expansion for all dates

The six variables to be considered as having the most influence on the expansion quantified by ε_V would be the coefficient of alkali fixation "FIXNA", the mortar porosity "POROMO", the initial concentration of alkali in cement paste "CNA0", the rim thickness "COLC(1)", the molar volume of ASR gel "VMGEL", and the Na_2O_{eq}/SiO_2 ratio "RNS".

4.3. Combined sensitivity analysis

In the previous parts, the sensitivity of the model has been analysed for each output. In this part, a combined sensitivity analysis is proposed in order to point out the parameters with the greatest influence on several outputs of interest. To obtain complete and precise analysis, it is based on five outputs that can, at various times in the course of the phenomenon and at various levels, impair the functionality of the dam:

- the total volume of gel formed for five time-steps,
- the corresponding ASR expansions,
- the expansion rate at the same five time-steps,

- the advancement of ASR in terms of expansion (5, 25, 50, 75, 90, 95, 100% of the final expansion),
- the time to reach the previous advancements.

In the following analysis, only cumulative frequency is presented. Using more outputs gives better precision in the evaluation. The ranking of input parameters obtained is presented in Fig. 10.

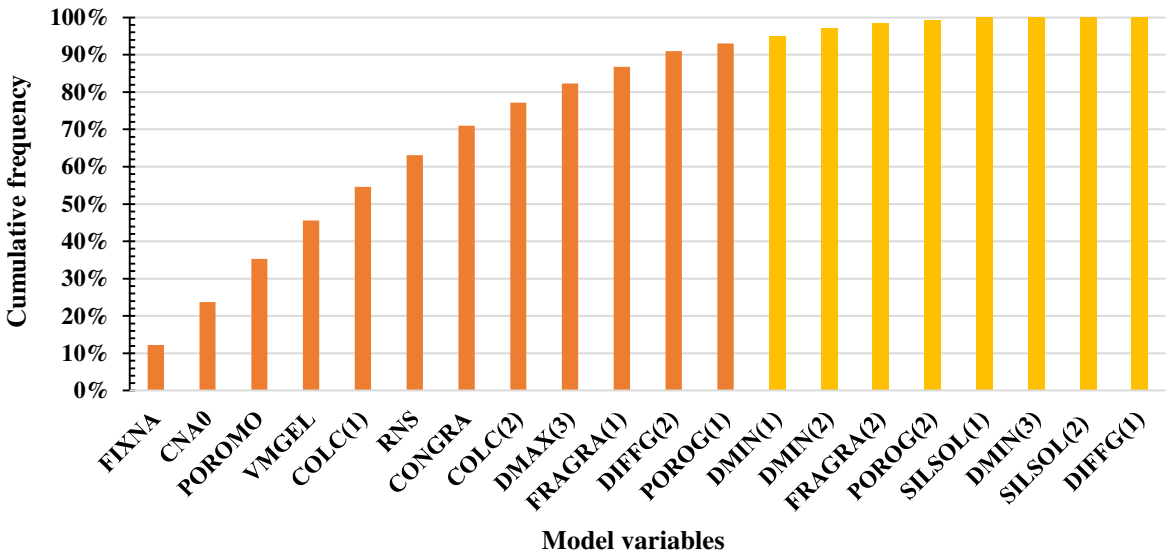

Fig. 10. Cumulative frequency on the sum of global sensitivity index of all outputs

The increase of cumulative frequency with the number of parameters is more progressive than in the previous analysis. This can be explained by the number of outputs taken into account here which, in turn, increases the number of possibly influential parameters, reaching 60% of the inputs.

The results confirm the prominence of the variable “FIXNA” compared to all the other variables for expansion tests at 38 °C. The initial concentration of alkali in cement paste, “CNA0”, which controls the attack range of aggregates, is the second most important parameter. This was not the case in the two first analyses where this parameter was the fourth then the third most influential parameter. All the other significant parameters of the two first analyses remain important in this cumulative analysis and only their relative rank can be modified from one output to another.

Fig. 10 shows that most of parameters have some impact on the outputs of the model. This analysis confirms the necessity to consider all the chemo-mechanical mechanisms quantified by these parameters. Finally, the parameters with little impact are mainly: the reactive silica content

(because, in these calculations, the limiting species are the alkali ions), the diffusion coefficient in the sand (as the sand particles are small, the diffusion is always fast in these particles) and the smallest size of the reactive particles (DMIN(i)).

5. Sensitivity analysis for ASR under environmental conditions

5.1. Impact of temperature on the sensitivity of the model

Due to the very wet environmental conditions of the Song Loulou dam (external relative humidity usually above 80%) and to the presence of the water intake, the concrete of the dam is assumed to be saturated. The aim of this part is thus to analyse the impact of the temperature on the sensitivity of the model.

5.2. Impact of constant in-field temperature on the sensitivity

The impact of the temperature on the sensitivity of the model is first analysed on expansions evaluated for a constant temperature of about 29 °C, which corresponds to the highest mean temperature recorded close to Song Loulou dam from 1975 to 2008 (Fig. 11). This temperature is lower than the temperature of the expansion test (38 °C) and can thus affect the importance of each parameter of the model. The cumulative frequency obtained for all the outputs is presented in Fig. 12.

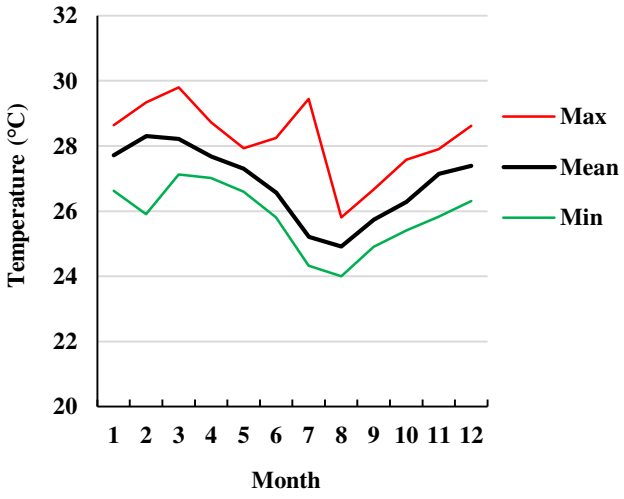

Fig. 11. Monthly mean temperature close to Song Loulou dam

The effect of a decrease of about 10 °C in the temperature is small (Fig. 12). The three most important parameters are the same (the alkali fixation, the initial alkali concentration and the mortar porosity). It is worth noting that the composition of ASR gels (through RNS, the Na_2O / SiO_2 ratio) is more important at 29 °C than at 38 °C (it gains two places in the ranking).

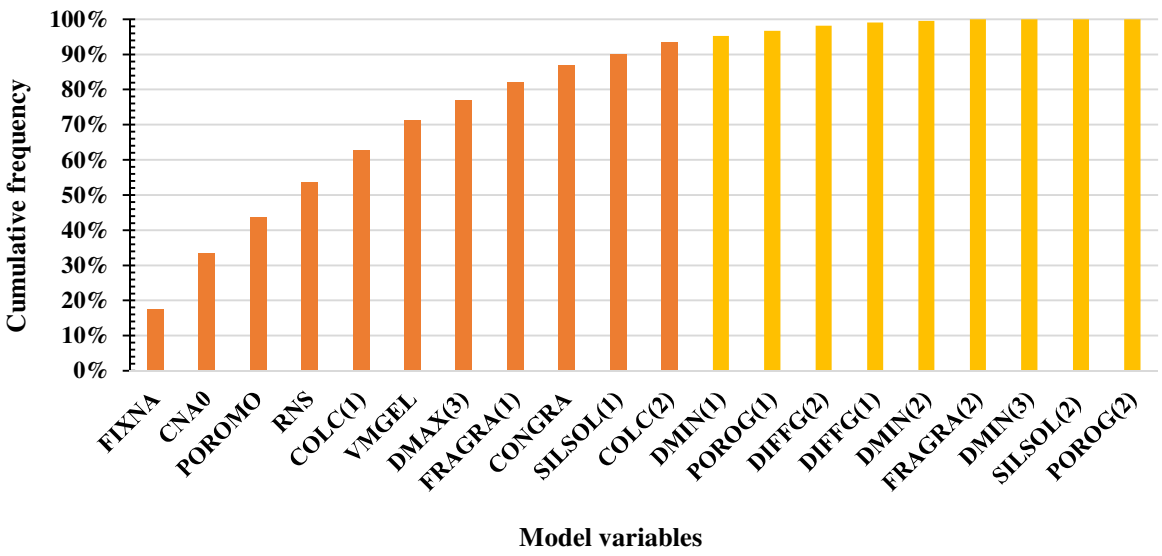

Fig. 12. Cumulative frequency on the sum of global sensitivity index of all outputs for a mean elevated temperature (29 °C, representative of the structure core)

To be useful for other structures damaged by ASR in other locations in the world, the effect of the temperature on the sensitivity of the model is secondly analysed on expansions evaluated for a lower constant temperature of about 10 °C. In this case, the temperature is about 30 °C lower than in the conditions of the expansion tests. A larger impact on the importance of each parameter can be expected. Fig. 13 highlights the ranking modification of the parameters. For this low temperature, the alkali concentration, CNA0, becomes the most important parameter and RNS, the ratio of Na_2O / SiO_2, becomes the second most important parameter for the first time in all the analyses.

The fixation of alkali, FIXNA, is still in fourth place. This confirms the importance of the kinetics of reactive mechanisms for the modelling of ASR expansion even at low temperature. It is also very interesting to note that, for low temperature, the reactive silica of the sand, SILSOL(1), is in sixth place. While it was not a limiting parameter for the laboratory expansion test, the importance of this parameter increases with decreasing temperature.

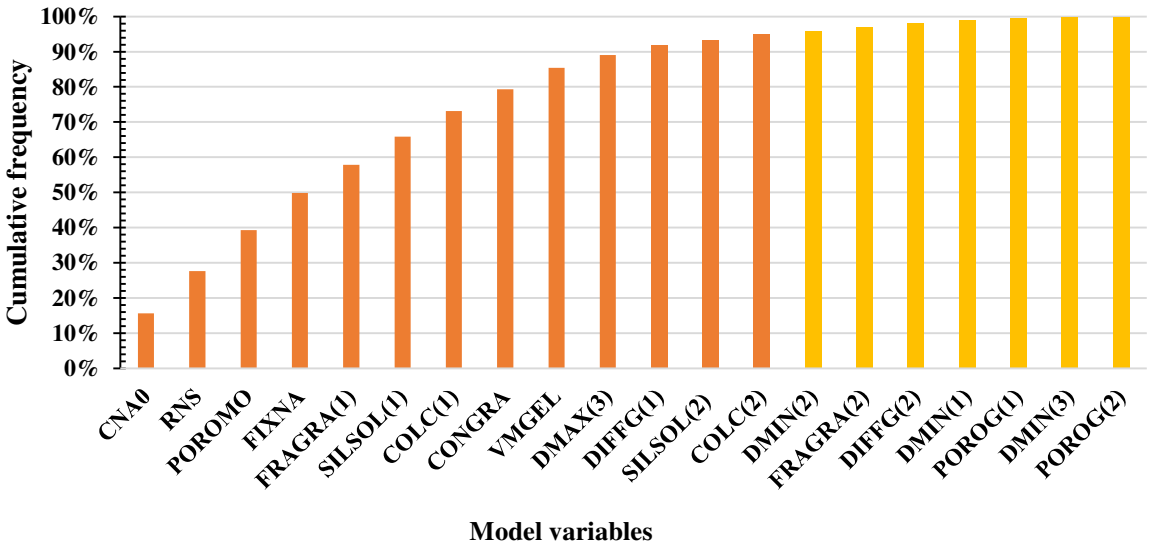

Fig. 13. Cumulative frequency on the sum of global sensitivity index of all outputs for a mean low temperature (10 °C, representative of the structure core)

5.3. Impact of variable temperature on the sensitivity

In large engineering structures such as dams, the core of the structure is little impacted by temperature cycles. Core temperature is almost constant. However, this is not the case for the skin of structures. Expansions induced at the skin are important as they can lead to deformation gradients and thus to cracking localized at the concrete skin. Such cracking can imply new paths for water into the structures and can cause new water supply able to accelerate ASR and thus the degradation of the structure.

Fig. 14 shows the cumulative analysis of the model for concrete subjected to the variable temperature conditions, representative of the skin of Song Loulou dam.

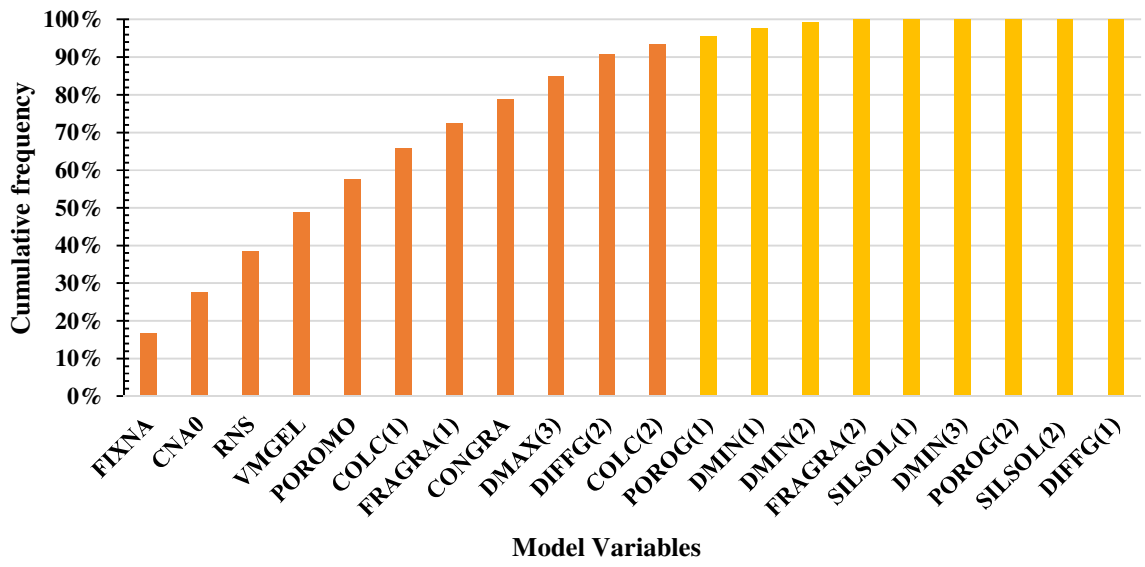

514

515 **Fig. 14.** Cumulative frequency on the sum of global sensitivity index of all outputs for variable
516 temperature conditions (representative of the skin of Song Loulou dam)

517 As the variation of temperature in the course of the year is small for Song Loulou dam (about 5
518 °C), the impact on the analysis is small in comparison with the analysis performed for a constant
519 temperature of 29 °C (Fig. 12). All the 11 important variables are the same for the two analyses.
520 However, even this small modification can impact the relative ranking of these important
521 variables. For example, the mortar porosity, POROMO, passes from the third place to the fifth,
522 while the Na_2O / SiO_2 ratio is more important for temperature cycling between 24 and 29 °C than
523 for the constant 29 °C. As the modification of kinetics with temperature follows an Arrhenius
524 exponential law, a small modification of temperature can lead to significant modifications of the
525 outputs.

526

527 ## 6. Discussion

528 6.1 Lessons learnt for ASR modelling at material scale

529 For all the sensitivity analyses performed in this work, the parameter, FIXNA, which quantifies
530 the impact of reactive mechanisms on ASR kinetics is of prime importance, while the coefficients
531 of diffusion in the aggregate, DIFFG(i), seem to have little effect (except for the volume of gel,
532 Vg, at 38 °C, Fig. 5 to Fig. 7). For all the situations, FIXNA is the most influential parameter,
533 except for expansion at low temperature (10 °C, Fig. 13 – but FIXNA is still ranked fourth).

534 This may seem surprising as a many models assume ASR kinetics to be controlled by alkali
535 diffusion in the aggregate. It is known that this assumption is realistic for aggregates with fast
536 reactivity, but not for certain slowly reacting aggregates, which present attacks distributed
537 throughout the aggregate and not an attack localized at aggregate edges [18,44,61]. Both transport
538 and the kinetics of chemical reactions have to be considered to obtain realistic representations of
539 all types of reactive aggregate (slow or fast reacting particles) [28,39].

540 To interpret the results of this analysis and, in particular, the impact of the parameter FIXNA, it is
541 important to note that the present study was carried out for data lying in the ranges found in
542 existing literature and defined in Table **1**. Thus, the coefficient of diffusion in aggregate was about
543 10^{-13} m²/s. It was measured through thin sections of quartzite aggregate in [47]. However, two
544 points are open to discussion. Firstly, coefficients of diffusion in aggregate are probably very
545 different from one rock to another (but few data on this type of measurements are available in the
546 literature). Secondly, the principle of the diffusion measurement used in [47] is not fully
547 representative of diffusion in ASR mechanisms: in [47], diffusion was evaluated through the time
548 necessary for alkali to cross the sample. This crossing can be partly achieved through connecting
549 paths. It does not mean that the aggregate is totally saturated in alkali. In the case of ASR, alkali
550 has to reach all the reactive silica in the aggregate. As aggregates come from natural,
551 heterogeneous material, diffusion is probably very different from one aggregate to another. The
552 principle of measurement used in [47] evaluates the diffusion at macro-scale but the coefficient of
553 diffusion in localized parts of the aggregate, representative of diffusion at micro scale, is probably
554 smaller and very heterogeneous in the particles. This highlights the importance of having reliable
555 experimental evaluations of all the parameters of the model if relevant sensitivity analysis is to be
556 obtained.

557 Moreover, the expansions studied here were obtained on an aged concrete extracted from a thirty-
558 year-old ASR-affected dam, while most of the ASR modelling in the literature is based on young
559 concrete cast and kept in laboratory conditions. In our case, the aggregate attack was not
560 homogeneous in the concrete at the beginning of the LPC N°44 accelerated test. In addition, as
561 ionic diffusion is first necessary to cause the chemical attack (hydroxyl ions have to move to
562 reactive silica to allow the dissolution), diffusion was probably more advanced than the chemical
563 attack of aggregate at the beginning of the test. This could have modified the relative impact
564 evaluated for the diffusion (DIFFG(i)) and the alkali fixation (FIXNA) on outputs during such
565 tests, and could thus explain why the parameter FIXNA is so prominent in the present analysis.

566 The second fruitful lesson learnt concerning the modelling of ASR at material scale is the
567 modification of the rank of parameters with the decrease of temperature. In particular, the
568 increasing influence of RNS, the Na_2O / SiO_2 ratio, with decreasing temperature should be noted.
569 In this modelling, this ratio was not directly modified by the temperature (but, as temperature acts
570 on equilibrium constants [27], this modification could improve the predictive capability of the
571 model); only the kinetics parameters (FIXNA and DIFFG) were impacted by temperature in the
572 present work. This means that the modification of the rank of RNS is a consequence of the
573 combination of different equations. At 38 °C, the kinetics of diffusion is very high, thus a large
574 proportion of the aggregates is rapidly saturated in hydroxyl and alkali. Ions are thus available in a
575 sufficient number of locations to produce ASR gel and thus expansion. For lower temperatures,
576 diffusion is slower. ASR gels can only be produced in a reduced number of locations. RNS, the
577 ratio of Na_2O / SiO_2, drives the number of moles of ASR gels that can be produced in a particular
578 location. One mole of SiO_2 leads to 1 mole of ASR gel: if the RNS is high, the gel is richer in
579 alkali. Alkali concentration has to be higher to produce the same quantity of gel. This is a
580 collateral consequence of the decrease of the kinetics rate by temperature.

581 In this work, the sensitivity analysis focused on the physico-chemical part of ASR modelling and
582 its impact of the kinetics of expansion. The mechanism of permeation of ASR gels through cracks
583 is not considered. At material scale, swelling tests are affected by the loss of ASR gel through
584 cracks resulting from expansion. Such loss of gels depends on the test temperature [62] but ASR
585 modelling has to consider the mechanical consequences of ASR, and particularly the cracks, to be
586 able to propose a reliable evaluation of this mechanism. In our approach, both ASR cracking and
587 anisotropic effects due to stress would be considered at structural scale in other numerical ways.

588

589 6.2 Lessons learnt for reliability ASR modelling at structural scale

590 Sensitivity analysis can be used to detect the most influential parameters for material modelling
591 and thus decrease the number of inputs if their impact is minimal. When structural modelling is
592 employed in a probabilistic context, only the major influential parameters have to be considered
593 random. The other parameters can be considered as deterministic since they have little influence
594 on the variability of outputs. This can help to avoid time-consuming calculations. Thus, resources
595 and efforts can be concentrated on improving the knowledge of leading parameters.

596 Combined analyses performed in the present paper point out that almost 60% of the parameters of
597 the model have significant influence on the results considering five outputs. For some particular

598 sensitivity analyses (gel volume or expansion), only 30% of the parameters have important effects.
599 For structural analysis, it is thus important to determine the most prominent outputs in order to
600 decrease the number of random parameters.

601 Temperature modifies the relative importance of ASR modelling parameters. For structural
602 condition assessment, some parameters can be calibrated on laboratory tests performed at 38 °C,
603 while the damaged structure is usually exposed to lower and fluctuating temperatures.
604 Consequently, the number of random parameters (the most influential ones) is increased for ASR
605 modelling for reliability in field conditions.

606 For the analysis of concrete already damaged by ASR (case of condition assessment of damaged
607 structures), 3 parameters amongst the most influential ones are the same for all the environmental
608 conditions: the coefficient of alkali fixation (FIXNA), the initial alkali concentration (CNA0) and
609 the porosity of the cement paste (POROMO). The molar volume of gel (VMGEL) and the reaction
610 rim thickness for small aggregates (COLC(1)) have major impacts on the output for laboratory
611 tests, while the ratio of Na_2O / SiO_2 of ASR gels (RNS) has a major impact in the temperature
612 conditions of Song Loulou dam. All these six parameters, at least, should be considered as random
613 for the reliability analysis of Song Loulou dam. For lower temperature, the fraction of the smallest
614 granular class of aggregates (FRAGRA(1)) also has an important impact (Fig. 13).

615 ## 7. Conclusion

616 A sensitivity analysis using the Morris method based on the ASR model developed at the material
617 scale in LMDC was carried out to reduce the stochastic dimension for a further reliability analysis.
618 Five outputs of the model were targeted: the total volume of gel, the ASR expansions, the
619 expansion rate, the advancement of ASR in terms of expansion and the time to reach this
620 advancement. A method to determine the most important parameters for multiple outputs using the
621 cumulative frequency of the sum of global sensitivity indices on all the outputs has been proposed
622 and applied not only time-wise but also over several times. Parameters were selected with a
623 cumulative frequency using a threshold value of 95%. Whatever the conditions, 60% of the
624 parameters have a major influence on all the outputs while only 30% of parameters affect a
625 particular output.
626 The parameters underlined as the most relevant in this sensitivity analysis are known to affect
627 ASR kinetics and expansion, even if they are not always taken into account in the models found in
628 the literature. In particular, the kinetics of reactive mechanisms are often ignored by models at the
629 material scale. This sensitivity study has shown that this may jeopardize the accuracy of the results

630 if they are used to analyse the expansion of cores drilled from damaged structures like the ones
631 used in the present work (coming from Song Loulou dam). It is also important to note the
632 dependency of the influential parameters on the temperature. The most significant parameters are
633 not the same for laboratory expansion tests at 38 °C and for real structures under low
634 temperatures. This points out the impact of the mechanisms quantified by these parameters and
635 their relative role according to temperature. A mechanism that is important at 38 °C can be
636 negligible at 10 °C. This explains why it is often so difficult to translate a conclusion obtained in
637 laboratory conditions to real structures.
638 In a probabilistic context, where the reliability analysis of dams exposed to ASR has to be
639 conducted, only the major parameters should be considered random for structural calculations.
640 The major parameters have to be determined for both temperatures if the model is calibrated on
641 laboratory tests and then used for structural assessment in field conditions. Future work should
642 assess the dam reliability [50].
643

644 **Credit authorship contribution statement**
645 **G. Ftatsi Mbetmi:** Conceptualization, Methodology, Programming, Results discussion, Writing –
646 original draft, Writing - review & editing. **S. Multon:** ASR modelling expertise, Methodology,
647 Results discussion, Writing - review & editing. **T. De Larrard:** Conceptualization, Methodology,
648 Results discussion, Writing - review & editing. **F. Duprat:** Conceptualization, Methodology,
649 Results discussion, Writing - review & editing, Supervision. **D. Tieudjo:** Writing - review &
650 editing, Supervision, computing resources.

651 **Declaration of competing interest**
652 None of the five authors have a conflict of interest.

653 **Acknowledgements**
654 The authors wish to thank the French Government for its financial support through its Department
655 of Cooperation and Cultural Action (SCAC) of the French Embassy in Cameroon.
656

Appendix A. Morris method and variable selection algorithm

Input: k, number of input variables ; X_{min}^{i} and X_{max}^{i}, minimum and maximum values of variables X_i with $i = 1, .., k$; p with $p > k$, the number of levels of each variation range; r, the number of trajectories, S_{thv}, sensitivity threshold value.

Output: Important variables

Begin

Initialize the lower triangular matrix $B_{(k+1)\times k}$

Initialize the matrix $J_{(k+1)\times k}$ of (k+1) lines and k columns, of ones

Initialize the diagonal matrix $D_{k\times k}^{*}$ whose diagonal terms randomly take the values 1 or -1

Initialize the matrix $P_{k\times k}^{*}$ such that each column and each line contain only one element equal to 1 and the others are equal to 0

Compute $\Delta = \frac{1}{p-1}$

Construct the levels vector $Vn[l] = \frac{l-1}{p-1}, l = 1, \dots, p$

for m=1 **to** r **do**

For each variable, randomly draw a value of Vn ; the set of k values obtained constitute the vector $X_{1\times k}^{*}$ of the coordinates of the initial point in the standard space.

Compute $B_{(k+1)\times k}^{*}$ using (Eq.4)

Compute $X^{j,i}, i = 1,2, \dots, k; j = 1,2, \dots, k+1$ using (Eq.5)

Compute $f(X_i)$ of each of $k+1$ points of the trajectory

Compute the elementary effects, $EE_i = \frac{f(X_{i+1})-f(X_i)}{\Delta}$, $i = 1,2, \dots, k$

end for

Compute the absolute means on r of the EE_i, μ_i^{*}

Compute the means and standard deviation on r of the EE_i, μ_i and σ_i

Compute the global sensitivity indices of each variable, S_i^{*} using (Eq.7)

if single output

Order S_i^{*} decreasingly and cumulate

Select variables with a cumulative S_i^{*} less than S_{thv}

else

For each variable, sum S_i^{*} on all outputs

Compute the frequencies on $\sum S_i^{*}$, order decreasingly, and cumulate

Select variables with cumulative frequencies less than S_{thv}

end if

End

References

[1] L.S. Dent Glasser, N. Kataoka, The chemistry of 'alkali-aggregate' reaction, Cem. Concr. Res. 11 (1981) 1–9. https://doi.org/10.1016/0008-8846(81)90003-X.

[2] A.B. Poole, Alkali-silica reactivity mechanisms of gel formation and expansion, in: 9th Int. Conf. Alkal-Aggreg. React., 1992: pp. 782–789.

[3] T.N. Jones, A new interpretation of alkali-silica reaction and expansion mechanism in concrete, Chem. Ind. (1988) 40–44.

[4] V.E. Saouma, M.A. Hariri-Ardebili, L. Graham-Brady, Stochastic analysis of concrete dams with alkali aggregate reaction, Cem. Concr. Res. 132 (2020) 106032.

[5] S. Multon, A. Sellier, M. Cyr, Chemo-mechanical modeling for prediction of alkali silica reaction (ASR) expansion, Cem. Concr. Res. 39 (2009) 490–500. https://doi.org/10.1016/j.cemconres.2009.03.007.

[6] L.F.M. Sanchez, S. Multon, A. Sellier, M. Cyr, B. Fournier, M. Jolin, Comparative study of a chemo–mechanical modeling for alkali silica reaction (ASR) with experimental evidences, Constr. Build. Mater. 72 (2014) 301–315. https://doi.org/10.1016/j.conbuildmat.2014.09.007.

[7] S.H. Paskov, J.F. Traub, Faster valuation of financial derivatives, J. Portf. Manag. 22 (1995) 113–123. https://doi.org/10.3905/jpm.1995.409541.

[8] R.E. Caflisch, W. Morokoff, A.B. Owen, Valuation of Mortgage Backed Securities Using Brownian Bridges to Reduce Effective Dimension, Department of Mathematics, University of California, Los Angeles, 1997. https://doi.org/10.1016/S0033-3506(49)81625-8.

[9] S. Kucherenko, B. Feil, N. Shah, W. Mauntz, The identification of model effective dimensions using global sensitivity analysis, Reliab. Eng. Syst. Saf. 96 (2011) 440–449. https://doi.org/10.1016/j.ress.2010.11.003.

[10] H.RIAHI, Analyse de structures à dimension stochastique élevée : application aux toitures bois sous sollicitation sismique, 2013.

[11] K. Bzowski, D. Bachniak, M. Pernach, M. Pietrzyk, Sensitivity analysis of phase transformation model based on solution of diffusion equation, Arch. Civ. Mech. Eng. 16 (2016) 186–192. https://doi.org/10.1016/j.acme.2015.10.004.

[12] P. Fasseu, Alcali-réaction du béton: Essai d'expansion résiduelle sur béton durci, Projet de méthode d'essai LPC No. 44, 1997.

[13] S. Multon, F.-X. Barin, B. Godart, F. Toutlemonde, Estimation of the Residual Expansion of Concrete Affected by Alkali Silica Reaction, J. Mater. Civ. Eng. 20 (2008) 54–62.

[14] C. Merz, A. Leemann, Assessment of the residual expansion potential of concrete from structures damaged by AAR, Cem. Concr. Res. 52 (2013) 182–189. https://doi.org/10.1016/j.cemconres.2013.07.001.

[15] R. Figueira, R. Sousa, L. Coelho, M. Azenha, J. de Almeida, P. Jorge, C. Silva, Alkali-silica reaction in concrete: Mechanisms, mitigation and test methods, Constr. Build. Mater. 222 (2019) 903–931.

[16] T. Guillemot, L. Lino, E. Nzalli, Diagnostic et mise en sécurité du barrage de Songloulou au Cameroun vis-vis des désordres liés à l'alcali-réaction., in: Colloq. Tech. Com. Fr. Barrages Réservoirs, 2013: pp. 153–162.

[17] A. Nielsen, F. Gottfredsen, F. Thøgersen, Development of stresses in concrete structures with alkali-silica reactions, Mater. Struct. 26 (1993) 152–158. https://doi.org/10.1007/BF02472932.

[18] C.F. Dunant, K.L. Scrivener, Micro-mechanical modelling of alkali-silica-reaction-induced degradation using the AMIE framework, Cem. Concr. Res. 40 (2010) 517–525. https://doi.org/10.1016/j.cemconres.2009.07.024.

[19] L. Charpin, A. Ehrlacher, Microporomechanics study of anisotropy of ASR under loading, Cem. Concr. Res. 63 (2014) 143–157. https://doi.org/10.1016/j.cemconres.2014.05.009.

[20] R. Esposito, M.A.N. Hendriks, A multiscale micromechanical approach to model the deteriorating impact of alkali-silica reaction on concrete, Cem. Concr. Compos. 70 (2016) 139–152. https://doi.org/10.1016/j.cemconcomp.2016.03.017.

[21] T. Iskhakov, J.J. Timothy, G. Meschke, Expansion and deterioration of concrete due to ASR : Micromechanical modeling and analysis, Cem. Concr. Res. 115 (2019) 507–518.

[22] A.B. Giorla, K.L. Scrivener, C.F. Dunant, Influence of visco-elasticity on the stress development induced by alkali–silica reaction, Cem. Concr. Res. 70 (2015) 1–8. https://doi.org/10.1016/j.cemconres.2014.09.006.
[23] Z.P. Bažant, G. Zi, C. Meyer, Fracture Mechanics of ASR in Concretes with Waste Glass Particles of Different Sizes, J. Eng. Mech. 126 (2000) 226–232. https://doi.org/10.1061/(ASCE)0733-9399(2000)126:3(226).
[24] I. Comby-Peyrot, F. Bernard, P.O. Bouchard, F. Bay, E. Garcia-Diaz, Development and validation of a 3D computational tool to describe concrete behaviour at mesoscale. Application to the alkali-silica reaction, Comput. Mater. Sci. 46 (2009) 1163–1177. https://doi.org/10.1016/j.commatsci.2009.06.002.
[25] S. Li, Z. Deng, C. Li, D. Chen, Y. Zhang, Modeling of flexural strength degradation induced by alkali-silica reaction, Constr. Build. Mater. 234 (2020) 117397.
[26] Y. Furusawa, H. Ohga, T. Uomoto, An analytical study concerning prediction of concrete expansion due to alkali–silica reaction, in: Malhotra Ed 3rd Int Conf Durab. Concr. Nice Fr., 1994: pp. 757–780, SP 145-40.
[27] T. Kim, J. Olek, Chemical sequence and kinetics of alkali-silica reaction part II. A thermodynamic model, J. Am. Ceram. Soc. 97 (2014) 2204–2212. https://doi.org/10.1111/jace.12830.
[28] V.E. Saouma, R.A. Martin, M.A. Hariri-Ardebili, T. Katayama, A mathematical model for the kinetics of the alkali–silica chemical reaction, Cem. Concr. Res. 68 (2015) 184–195. https://doi.org/10.1016/j.cemconres.2014.10.021.
[29] W. Grymin, D. Gawin, M. Koniorczyk, Experimental and numerical investigation of the alkali-silica reaction in the cement-based materials, Arch. Civ. Mech. Eng. 18 (2018) 1698–1714. https://doi.org/10.1016/j.acme.2018.07.003.
[30] Z.P. Bazant, A. Steffens, Mathematical model for kinetics of alkali-silica reaction in concrete, Cem. Concr. Res. 30 (2000) 419–428. https://doi.org/10.1016/S0008-8846(99)00270-7.
[31] B. Li, Z.-R. Wang, H.-B. Liu, X.-Z. Liu, H. Li, X. Chen, Meso-mechanical research on alkali-silica reaction expansion in Pyrex glass and silica sand at different temperatures and curing times, Constr. Build. Mater. 223 (2019) 377–393.
[32] A. Sellier, J.P. Bournazel, A. Mébarki, Une modélisation de la réaction alcalis-granulat intégrant une description des phénomènes aléatoires locaux, Mater. Struct. 28 (1995) 373–383. https://doi.org/10.1007/BF02473072.
[33] A. Suwito, W. Jin, Y. Xi, C. Meyer, A Mathematical Model for the Pessimum Size Effect of ASR in Concrete, Concr. Sci. Eng. 4 (2002) 23–34.
[34] S. Poyet, A. Sellier, B. Capra, G. Foray, J.-M. Torrenti, H. Cognon, E. Bourdarot, Chemical modelling of Alkali Silica reaction: Influence of the reactive aggregate size distribution, Mater. Struct. 40 (2007) 229–239. https://doi.org/10.1617/s11527-006-9139-3.
[35] M. Alnaggar, G. Cusatis, G. Di Luzio, Lattice Discrete Particle Modeling (LDPM) of Alkali Silica Reaction (ASR) deterioration of concrete structures, Cem. Concr. Compos. 41 (2013) 45–59. https://doi.org/10.1016/j.cemconcomp.2013.04.015.
[36] C. Qian, Y. Zhuang, H. Huang, Numerical calculation of expansion induced by alkali silica reaction, 103 (2016) 117–122.
[37] Y. Takahashi, S. Ogawa, Y. Tanaka, K. Maekawa, Scale-Dependent ASR Expansion of Concrete and Its Prediction coupled with Silica Gel Generation and Migration, J. Adv. Concr. Technol. 14 (2016) 444–463. https://doi.org/10.3151/jact.14.444.
[38] B. Li, L. Baingam, K. Kurumisawa, T. Nawa, L. Xiaozhou, Micro-mechanical modelling for the prediction of alkali-silica reaction (ASR) expansion : Influence of curing temperature conditions, 164 (2018) 554–569.
[39] S. Multon, A. Sellier, Multi-scale analysis of alkali-silica reaction (ASR): Impact of alkali leaching on scale effects affecting expansion tests, Cem. Concr. Res. 81 (2016) 122–133. https://doi.org/10.1016/j.cemconres.2015.12.007.

[40] T. Kim, J. Olek, H. Jeong, Alkali–silica reaction: Kinetics of chemistry of pore solution and calcium hydroxide content in cementitious system, Cem. Concr. Res. 71 (2015) 36–45. https://doi.org/10.1016/j.cemconres.2015.01.017.
[41] L. Charpin, A. Ehrlacher, A computational linear elastic fracture mechanics-based model for alkali-silica reaction, Cem. Concr. Res. 42 (2012) 613–625. https://doi.org/10.1016/j.cemconres.2012.01.004.
[42] M. Alnaggar, G. Di Luzio, G. Cusatis, Modeling Time-Dependent Behavior of Concrete Affected by Alkali Silica Reaction in Variable Environmental Conditions, (2017) 1–32.
[43] C. Qian, Y. Zhuang, H. Huang, Numerical calculation of expansion induced by alkali silica reaction, Constr. Build. Mater. 103 (2016) 117–122.
[44] J.M. Ponce, O.R. Batic, Different manifestations of the alkali-silica reaction in concrete according to the reaction kinetics of the reactive aggregate, Cem. Concr. Res. 36 (2006) 1148–1156. https://doi.org/10.1016/j.cemconres.2005.12.022.
[45] T. Ichikawa, Alkali-silica reaction, pessimum effects and pozzolanic effect, Cem. Concr. Res. 39 (2009) 716–726. https://doi.org/10.1016/j.cemconres.2009.06.004.
[46] X.X. Gao, S. Multon, M. Cyr, A. Sellier, Alkali-silica reaction (ASR) expansion: Pessimum effect versus scale effect, Cem. Concr. Res. 44 (2013) 25–33.
[47] S. Goto, D.M. Roy, Diffusion of ions through hardened cement pastes, Cem. Concr. Res. 11 (1981) 751–757.
[48] D. Bulteel, E. Garcia-Diaz, C. Vernet, H. Zanni, Alkali–silica reaction: A Method to quantify the reaction degree, Cem. Concr. Res. 32 (2002) 1199–1206. https://doi.org/10.1016/S0008-8846(02)00759-7.
[49] S. Multon, A. Sellier, E. Grimal, E. Bourdarot, Structures damaged by ASR and DEF: Improving the prognosis of structures damaged by expansive concrete with physico-chemical modelling, in: Swelling Concr. Dams Hydraul. Struct. DSC 2017, Wiley, 2017.
[50] G. Ftatsi Mbetmi, Fiabilité résiduelle des ouvrages en béton dégradés par réaction alcali-granulat: application au barrage hydroélectrique de Song Loulou, PhD Thesis, Université de Toulouse, Université Toulouse III-Paul Sabatier, 2018.
[51] J. Lindgård, M.D. Thomas, E.J. Sellevold, B. Pedersen, Ö. Andiç-Çakır, H. Justnes, T.F. Rønning, Alkali–silica reaction (ASR)—performance testing: influence of specimen pre-treatment, exposure conditions and prism size on alkali leaching and prism expansion, Cem. Concr. Res. 53 (2013) 68–90.
[52] F. De Larrard, Concrete mixture proportioning: a scientific approach, CRC Press, 1999.
[53] X.X. Gao, Contribution to the requalification of ASR-damaged structures: Assessment of the ASR advancement in aggregates, PhD Thesis, 2010.
[54] H.F.W. Taylor, Cement chemistry, Thomas Telford, 1997.
[55] R.Y. Rubinstein, D.P. Kroese, Simulation and the Monte Carlo Method, John Wiley & Sons, 2011.
[56] I. Sobol, A primer for the Monte Carlo method, (1994).
[57] M.D. Morris, Factorial Sampling Plans for Preliminary Computational Experiments, Technometrics. 33 (1991) 161. https://doi.org/10.2307/1269043.
[58] F. Campolongo, J. Cariboni, A. Saltelli, An effective screening design for sensitivity analysis of large models, Model. Comput.-Assist. Simul. Mapp. Danger. Phenom. Hazard Assess. 22 (2007) 1509–1518. https://doi.org/10.1016/j.envsoft.2006.10.004.
[59] D.M. King, B.J.C. Perera, Morris Method of sensitivity analysis applied to assess the importance of input variables on urban water supply yield--a case study, J. Hydrol. 477 (2012) 17–32. http://dx.doi.org/10.1016/j.jhydrol.2012.10.017.
[60] I. Sobol, A. Gresham, On an alternative global sensitivity estimator, Proc. SAMO. (1995) 40–42.
[61] M. Ben Haha, E. Gallucci, A. Guidoum, K.L. Scrivener, Relation of expansion due to alkali silica reaction to the degree of reaction measured by SEM image analysis, Cem. Concr. Res. 37 (2007) 1206–1214. https://doi.org/10.1016/j.cemconres.2007.04.016.
[62] Y. Kawabata, C. Dunant, K. Yamada, K. Scrivener, Impact of temperature on expansive behavior of concrete with a highly reactive andesite due to the alkali–silica reaction, Cem. Concr. Res. 125 (2019) 105888.